Crystal and electronic structure of $Li_{15}Si_4$

Yoshiyuki Kubota
Department of Precision Science and Technology and Applied Physics, Osaka University, Suita, Osaka 565-0871, Japan and Power Engineering Research and Development Center, Research and Development Department, Kansai Electric Power Company, Inc., Amagasaki, Hyogo 661-0974, Japan

Mary Clare Sison Escaño, Hiroshi Nakanishi, and Hideaki Kasai
Department of Precision Science and Technology and Applied Physics, Osaka University, Suita, Osaka 565-0871, Japan

(Received 21 May 2007; accepted 14 July 2007; published online 6 September 2007)

Silicon is one of the most promising anode materials for future rechargeable batteries because of its high theoretical capacity. New crystalline $Li_{15}Si_4$ was found as the fully electrochemical lithiated phase of crystalline Si or amorphous Si. Density functional theory was used to study the crystal and electronic structure of $Li_{15}Si_4$. $Li_{15}Si_4$ is formed by the unit figure in which six Li atoms surround a Si atom with two different Li–Si bond lengths. The Li atom has negative charge of 0.56–0.63 in $Li_{15}Si_4$. The average intercalation voltage for the lithium intercalation reaction from crystalline Si to $Li_{15}Si_4$ is 0.303 V, which is in good agreement with that predicted by the Coulometric titration experiment result for Li–Si alloys. © *2007 American Institute of Physics*.
[DOI: 10.1063/1.2775999]

I. INTRODUCTION

Lithium-ion batteries (LIBs) are widely used as the current rechargeable power source for portable electronics devices such as laptop computers and cellular telephones.[1] Compared to conventional secondary batteries, such as lead-acid, nickel–cadmium, and nickel–metal hydride, LIBs have higher energy density, higher operating voltages, and lower self-discharge.[1,2] Further increase in the energy density and in thermal stability of LIBs may lead to potential use for aerospace, military, and automobile applications.

For anodes of LIBs, the conventional material is graphite[1,3] with a theoretical specific capacity of 372 mA h/g-C_6(840 A h/L-C_6). Alternative anode materials with higher capacity are needed to increase the specific energy of LIBs. Some of the most promising materials include silicon (Si), tin (Sn), and alloys containing these elements.[1] In particular, Si has a large theoretical specific capacity of 4008 mA h/g-Si(9339 A h/L-Si), more than 10-fold greater than that of graphite.[4,5] In addition, Si is the second most abundant element in the earth's crust. Due to its very high theoretical Li accommodation capacity, Si has been studied extensively as an anode material for next-generation Li-ion batteries.[6–9] However, in spite of its high theoretical capacity, Si anodes do not retain their capacity over a large number of cycles.[1] The cycling behavior of crystalline Si shows a fall below 50% of its initial capacity after less than several cycles of charge/discharge. This poor cycle performance is believed to be due to the big volume change during Li intercalation/deintercalation, which inevitably causes great stress in the Si lattice, and thus leads to cracking and crumbling of the Si particle.[1] As a result, the capacity for alloying Li fades abruptly only after several cycles.

It is necessary to study the Li–Si system fundamentally to overcome the problems with its poor cycle performance. Recently some studies have shown that crystalline Si becomes amorphous upon alloying with lithium during Li intercalation reaction.[10–14] Obrovac *et al.* reported that there is first a two-phase region due to the conversion of crystalline Si to partially lithiated amorphous Si during the discharge, and the amorphous Li–Si alloy suddenly crystallizes into the $Li_{15}Si_4$ phase below 50 mV versus Li.[12] Their x-ray diffraction (XRD) result revealed that the fully lithiated phase of Si at room temperature is not $Li_{21}Si_5$ as is widely believed, but $Li_{15}Si_4$. The theoretical specific capacity for this phase is about 3579 mA h/g-Si, which more closely agrees with their experimental results. A similar result was reported for amorphous Si anodes by Hatchard *et al.*[15] They reported that amorphous Si films thicker than 2.5 μm crystallize to form a crystalline $Li_{15}Si_4$ phase below 30 mV versus Li and a 0.5 μm thick amorphous Si film never crystallized. Limthongkul *et al.* showed the conversion of a crystalline Si into the amorphous Li–Si alloy by using XRD and high-resolution electron microscopy (HREM).[13,14] They claim that a Si sample lithiated to $Li_{2.17}Si$ is the coexistence of an amorphous phase with crystalline Si due to decrease of the Si peaks.[14] The XRD results of $Li_{2.17}Si$ also showed small broad peaks at 2θ=39.4°, 41.3°, and 43.1°. Their peaks were not identified by Limthongkul *et al.* in detail, but we think that the $Li_{2.17}Si$ phase they obtained contains $Li_{15}Si_4$ from the XRD results reported by Obrovac *et al.*[12] or Hatchard *et al.*[15]

It is well known that the Li–Si phase diagram offers a rich variety of solid crystalline compounds.[16,17] Crystalline compounds exist with the compositions $Li_{21}Si_5$,[18] $Li_{13}Si_4$,[19] $Li_{14}Si_6$,[20] $Li_{12}Si_7$,[21,22] and LiSi,[23,24] However, these compounds do not appear in electrochemical Li intercalation/deintercalation of crystalline Si.[12–14] This feature is sharply different from the case of tin (Sn) anodes of LIBs. The beginning and end of the plateaus of discharge profile for the Sn anode approximately corresponds to the Li–Sn phase diagram.[25,26]

We think that the Li–Si compounds as shown in Li–Si phase diagram[16,17] are thermodynamically the most stable states since they are obtained at a high temperature of about 688 K. We think that the electrochemical stable states at room temperature may not fall into the thermodynamically most stable states but into metastable states: they may be amorphous Li–Si alloys and crystalline $Li_{15}Si_4$ in the plateau region in the Li–Si system.

At the start of study on the lithium intercalation reaction of Si anodes, it is important to elucidate the electronic structure of the crystalline $Li_{15}Si_4$ phase formed at the end of the plateaus of discharge for crystalline Si and amorphous Si. In this study, we investigate the crystal geometric structure, electronic structure, charge density distribution, and density of states (DOS) of $Li_{15}Si_4$ by implementing density functional theory (DFT) calculations.

Next, we calculate the average intercalation voltage for the Li–Si system to evaluate the electrochemical validity of DFT calculations. Aydinol *et al.* showed the average voltages of some metal oxides for cathodes of LIB by using the DFT calculations and basic thermodynamics.[27,28] Courtney *et al.* applied Aydinol *et al.*'s method to the Li–Sn system to calculate the electrochemical voltage profile.[29] The calculated voltage profile lies between the curves obtained by the charge–discharge test. Unlike the electrochemical Li–Sn system[29] in which multiple crystalline phase regions appear in the Li–Sn phase diagram,[4] the crystalline phase of electrochemical lithiated Si is only the $Li_{15}Si_4$ phase.[12] Therefore, the electrochemical voltage profile for the Li–Si system is not the curve, but the constant value calculated from the total energy difference between the sum of metallic Li and crystalline Si and $Li_{15}Si_4$. We confirmed our calculation on the average intercalation voltage using Coulometric titration experiment results.[26]

The average intercalation voltage is derived from integrating the chemical potential difference in the anode and cathode, and associated with the Gibbs free energy obtained by DFT calculations, that is, the Nernst equation. This voltage represents the equilibrium voltage (no load) and does not account for resistivity effects or overpotentials when current is drawn. In evaluation of the structures of intermediates during the electrochemical reaction, it is important to estimate this voltage since it approximately expresses the open circuit voltage (OCV) when the electrodes are partially lithiated.

Assuming that a cathode is Li_xSi and an anode is metallic Li, the lithium intercalation reaction formula during the discharge is expressed by

$$Li_xSi + (y-x)Li \rightarrow Li_ySi, \tag{1}$$

where $y-x$ is the charge on the lithium ion in the electrolyte $(y>x)$.

By applying the method in Refs. 27 and 28 to reaction (1), the average intercalation voltage, $\bar{V}$, is given by

$$\bar{V} = -\frac{\Delta G_r}{(y-x)F}, \tag{2}$$

where F is Faraday's constant and ΔG_r is the Gibbs free energy change in reaction (1).

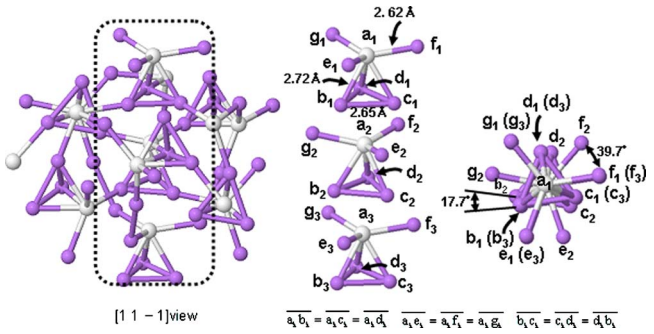

FIG. 1. (Color online) Crystal structure for $Li_{15}Si_4$. The white spheres are the Si atoms, and the gray spheres are the Li atoms. The left figure is view along [11−1]. The middle figure shows simple layer structures by extracting the part framed in by the dot line in the left figure. The symbols b_k, c_k, d_k, e_k, f_k, and g_k are locations of the Li atoms, and a_k is a location of the Si atoms, where $k=1,2,3,\ldots$. The right figure shows the overhead view of middle figure. The parentheses in the right figure express the overlap.

Equation (2) allows one to compute the average voltage between Li_xSi and Li_ySi. Calculations can be significantly simplified by further approximating $\Delta G_r = \Delta E_r + P\Delta V_r - T\Delta S_r$ by the change in internal energy (ΔE_r) at 0 K. The term $P\Delta V_r$ is of the order of 10^{-5} electron volts, whereas the term $T\Delta S_r$ is of the order of the thermal energy.[27,28] The above approximation is good since ΔE_r is of the order of 0.1 eV per molecule for Si materials. By applying these simplifications, we obtain

$$\bar{V} = \frac{E_r[Li_xSi] + (y-x)E_r[Li] - E_r[Li_ySi]}{(y-x)F}. \tag{3}$$

II. COMPUTATIONAL DETAILS

We used DFT calculations within the generalized gradient approximation (GGA) for the exchange-correlation functional using ultrasoft pseudopotentials[30,31] as implemented in the Vienna Ab Initio Simulation Package (VASP).[32–35] The Perdew–Burke–Ernzerhof (PBE) functional[36,37] has been adopted for the GGA. The full potential for the Li atom was used. An energy cutoff of 271.6 eV was used to expand the plane-wave basis. The 60 Li atoms and 16 Si atoms are ordered in a unit cell for $Li_{15}Si_4$ in consideration in the space group of $Li_{15}Si_4$, $I\bar{4}3d$.

An $11\times11\times11$ k-point mesh was used for calculations of $Li_{15}Si_4$. All structure relaxations were performed by conjugate-gradient (CG) (Refs. 38 and 39) optimization for atomic coordinates to minimize the total energy. All the calculations performed here were nonspin polarized.

III. RESULTS AND DISCUSSIONS

A. Crystal structure

We start our discussion by analyzing the structures of $Li_{15}Si_4$. The crystalline structure for $Li_{15}Si_4$ is illustrated in Fig. 1. The white spheres are the Si atoms, and the gray spheres are the Li atoms. The left figure in Fig. 1 is the view along [11−1]. Each Si atom is connected to six other neighboring Li atoms forming one unit figure. The links between these figures seem to be complex but are just made of simple layer structures extracted by the part framed in by the dotted

TABLE I. Lattice constant and fractional coordinates of $Li_{15}Si_4$. The space group is $I\bar{4}3d$.

Parameter	Calc (This work)	Expt (Ref. 12)	Expt (Ref. 15)
Lattice constant	10.60	10.6852(9)	10.777
Li(12a) (x,y,z)	(0.375, 0.000, 0.250)	(0.375, 0.000, 0.250)	(0.375, 0, 0.25)
Li(48e) (x,y,z)	(0.123, 0.154, 0.963)	[0.118(1), 0.156(1), 0.961(1)]	(0.130, 0.177, 0.865)
Si(16c) (x,y,z)	(0.458, 0.458, 0.458)	[0.4588(2), 0.4588(2), 0.4588(2)]	(0.462, 0.462, 0.462)

line in the left figure, as shown in the middle figure in Fig. 1. The symbols, b_k, c_k, d_k, e_k, f_k, and g_k are locations of the Li atoms, and a_k is a location of the Si atoms, where $k=1,2,3\ldots$. It was found that $Li_{15}Si_4$ is formed by the series of such unit figures of six Li atoms surrounding a Si atom with two Li–Si bond lengths of 2.62 Å ($a_kb_k=a_kc_k=a_kd_k$) and 2.72 Å ($a_ke_k=a_kf_k=a_kg_k$). By using the calculated Li–Li bond length of 2.97 Å in metallic Li and the calculated Si–Si bond length of 2.37 Å in crystalline Si, the calculated average Li–Si bond length was 2.67 Å, which is between the abovementioned Li–Si bond lengths in $Li_{15}Si_4$. The Li–Li bond length of the equilateral triangle of $b_kc_kd_k$ is 2.65 Å, which is much shorter than the calculated Li–Li bond length of 2.97 Å in metallic Li. We attribute the short Li–Li bond length in $Li_{15}Si_4$ to Li atoms being forced to cage in the Li–Si alloy cavities.

The series of the unit figures intricately intersect with other series of unit figures, as shown in the left figure in Fig. 1. The Li atom of a unit figure, the point of e, f, or g, is equal to the point of b, c, or d of other unit figures.

The unit figure marked by an odd number suffix and that marked by an even number suffix are similar but not completely congruent figures, as will be shown later. The planes passing through three points of b_k, c_k, and d_k are parallel to that passing through three points of e_k, f_k, and g_k. The right figure in Fig. 1 shows the top view of the middle figure. The parentheses in the right figure show that the symbols overlap with the symbols in parentheses. The projected line of b_1c_1, c_1d_1, and d_1b_1 onto the plane of the $b_2c_2d_2$ intersect with the line of b_2c_2, c_2d_2, and d_2b_2 at an angle of 17.7°. Similarly, the projected line of a_1e_1, a_1f_1, and a_1g_1 onto the plane of the $e_2f_2g_2$ intersect with the line of a_2e_2, a_2f_2, and a_2g_2 at an angle of 39.7°. It was found that a unit marked by an odd suffix and that marked by an even suffix are not congruent. The distance between the point of a_k and the plane of $e_kf_kg_k$ is 0.34 Å. The distance between the point of a_k and the plane of $b_kc_kd_k$ is 2.24 Å. The distance between the plane of $b_kc_kd_k$ and that of $e_{k+1}f_{k+1}g_{k+1}$ is 2.01 Å. It was also found that unit figures lie in a straight line in the periodic length of 4.59 Å along the axis of a_1a_k. The base of a triangular pyramid of $a_kb_kc_kd_k$ is an equilateral triangle of $b_kc_kd_k$ made of three Li atoms.

Table I gives lattice constants and fractional coordinates of $Li_{15}Si_4$. The "Calc" and "Expt" lines give the calculated parameters in this work and the experimental parameters determined by XRD, respectively.[12,15] The second line is the *ex situ* XRD data from the fully lithiated crystalline Si,[12] and the third line is the *in situ* XRD data from the fully lithiated amorphous Si.[15] The calculated parameters are in better agreement with the *ex situ* XRD data than the *in situ* XRD data. This is because the *in situ* XRD data have errors by influence of a Be window in the *in situ* XRD cell and reflections from other cell parts as they described.[15]

B. Electronic structure

Next, we calculate the ionic charges of Li and Si in $Li_{15}Si_4$ by using the Wigne–Seitz radii of metallic Li and crystalline Si. The Wigner–Seitz radii is 1.814 Å for metallic Li and 1.5765 Å for crystalline Si from the calculation results in Ref. 40. Table II shows the numbers of valence electrons of the Li atom in metallic Li, the Si atom in crystalline Si, and the Li and Si atoms in $Li_{15}Si_4$.[40] The ranges of the number of valence electrons of Li–Si are due to the maximum and minimum electrons in all of Li atoms and Si atoms. The number of valence electrons within the Li atom region in $Li_{15}Si_4$ was estimated to be 1.56–1.63 electrons within the Wigner–Seitz radius of 1.814 Å. Therefore, we think that the Li atom in $Li_{15}Si_4$ is an anion with an excess charge of 0.56–0.63. Similarly, the number of electrons within the Si atom region in $Li_{15}Si_4$ was estimated to be 3.51–3.55 electrons within the Wigner–Seitz radius of 1.5765 Å. Therefore, we think that the Si atom in $Li_{15}Si_4$ is a cation with a positive charge of 0.45–0.49. There is no obvious change in the s electrons of the Li atoms between metallic Li and $Li_{15}Si_4$. Similarly, there is no change in the s electrons of the Si atoms between crystalline Si and Li–Si. Compared to the numbers of electrons in the Li atoms of metallic Li and $Li_{15}Si_4$, an increase of p and d electrons mainly contributes to the formation of Li anions in $Li_{15}Si_4$. In contrast, compared to the numbers of electrons in the Si atoms of crystalline Si and $Li_{15}Si_4$, a decrease of p and d electrons mainly contributes to the decrease of electrons in Si. We attribute the appearance of Li $3d$ electrons with the very high energy in $Li_{15}Si_4$ to tails of Si-based wave functions showing d symmetry on a Li site because of the crystal symmetry. The negatively charged Li atom also appears from the DFT cal-

TABLE II. Number of electrons of Li and Si in metallic Li, crystalline Si, and $Li_{15}Si_4$.

	Li		Si	
	Metallic Li[40]	$Li_{15}Si_4$	Crystalline Si [40]	$Li_{15}Si_4$
S	0.48	0.48–0.53	1.37	1.37
p	0.48	0.88–0.90	2.34	2.11–2.15
d	0.04	0.20–0.21	0.29	0.03
Total	1.00	1.56–1.63	4.00	3.51–3.55

TABLE III. Charge density distribution of metallic Li and the Li–Li bonds in $Li_{15}Si_4$. The first column starting from left is for metallic Li. The second column is for the unit figure of $a_1b_1c_1d_1e_1f_1g_1$ in $Li_{15}Si_4$. The figures in the second line from the top indicate the body-centered-cubic lattice of metallic Li and the unit figure in $Li_{15}Si_4$. The symbols a, b, c, b_1, c_1, d_1, e_1, f_1, and g_1 are locations of the Li atoms, and a_1 is a location of the Si atom (see the middle figure of Fig. 1). The shaded portion in each figure indicates the plane to depict the charge-density map. The maps in the third line from the top indicate the charge density distributions corresponding to the shaded portions in the second line. The fourth and fifth lines from the top indicate the ranges and intervals, respectively.

Compound	Metallic Li	$Li_{15}Si_4$
Structure	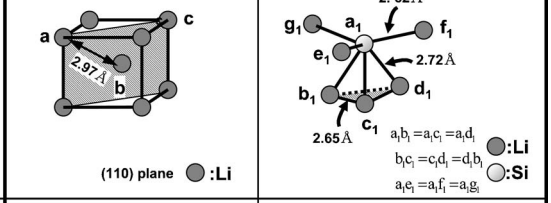	
Map	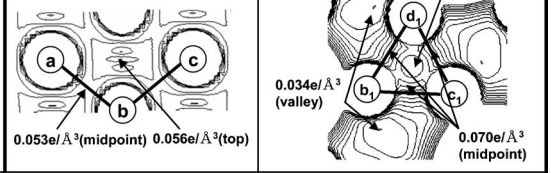	
Range	0.052 ~ 0.056 e/Å³	0.034 ~ 0.082 e/Å³
Interval	0.001 e/Å³	0.004 e/Å³

culations of LiSi and Li_6Si_5. The Li atom has an excess charge of 0.83–0.84 electrons for LiSi (Ref. 40) and 0.9 electrons for Li_6Si_5.[41]

The charge density distribution of metallic Li and the Li–Li bonds in $Li_{15}Si_4$ are shown in Table III. The first column starting from the left is for metallic Li, which is quoted from Ref. 40. The second column is for the unit figure of $a_1b_1c_1d_1e_1f_1g_1$ in $Li_{15}Si_4$. The figures in the second line from the top indicate the bcc lattice of metallic Li and the unit figure in $Li_{15}Si_4$. The symbols, a, b, c, b_1, c_1, d_1, e_1, f_1, and g_1 are locations of the Li atoms, and a_1 is a location of the Si atom (see the middle figure of Fig. 1). The shaded portion in each figure indicates the plane to depict the charge density map. The maps in the third line from the top indicate the charge density distributions corresponding to the shaded portions in the second line. The fourth and fifth lines from the top indicate the ranges and intervals, respectively. First, we observe the charge density map of metallic Li. The electrons in metallic Li are mainly concentrated around the Li atom as characterized by its s orbital. Therefore, the charge density at the midpoint of the Li–Li bond is 0.053 electrons/Å^3. We subsequently examine the charge density map of an equilateral triangle of $b_1c_1d_1$ made of three Li atoms in $Li_{15}Si_4$. The charge densities at the midpoints of three Li–Li bonds (b_1c_1, c_1d_1, and d_1b_1) are 0.070 electrons/Å^3, which is higher than that for the Li–Li bond in metallic Li. The maximum charge density is 0.081 electrons/Å^3 at the center of an equilateral triangle of $b_1c_1d_1$. The formation of the Li anions in $Li_{15}Si_4$ is due to the increase of the charge density at the midpoint of the Li–Li bond or at the gravity point of three Li atoms.

TABLE IV. Charge density distribution of the L–Si bonds in $Li_{15}Si_4$. The view of the figures and the symbols of this table are the same as in Table III.

Compound	$Li_{15}Si_4$
Structure	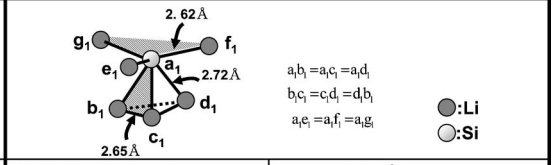
Map	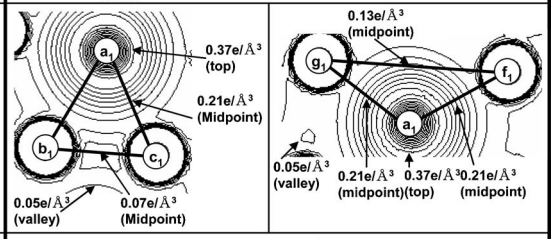
Range	0.05 ~ 0.37 e/Å³
Interval	0.04 e/Å³

The charge density distributions of the Li-Si bonds in $Li_{15}Si_4$ are shown in Table IV. The first column starting from the left is for a triangle of $a_1b_1c_1$. The second column is for a triangle of $a_1f_1g_1$. The view of the figures and the symbols of Table IV are the same as Table III. The charge density distributions at the midpoints of three Li–Si bonds (a_1b_1, a_1c_1, and a_1d_1) are the same, 0.21 electrons/Å^3. Similarly, the charge density distributions at the midpoints of another three Li–Si bonds (a_1e_1, a_1f_1, and a_1g_1) are the same, 0.21 electrons/Å^3. The charge densities are concentrated around the Si atoms when looking at the Li–Si bonds. We think that electrons in $Li_{15}Si_4$ are mainly located very close to the Si atoms due to electronegativity. The charge densities at the bonding midpoints of the Li–Si bonds are also higher than those in Li–Li bond in metallic Li. From the viewpoint of the Li atom, the Si atom-derived electrons come in proximity to the Li atoms. We think that these electrons contribute to the formation of the Li anions. These results resemble the calculated results of LiSi in the charge density distributions of the Li–Si bonds.[40]

The total DOS curve for $Li_{15}Si_4$ is presented in Fig. 2. The energy scale is relative to the Fermi level (E_F). The band gap near E_F of crystalline Si vanishes and a new band gap between −1.3 eV and −4.9 eV appears. A similar band gap in the DFT calculation for $Li_{12}Si_7$ is reported.[41]

Figure 3 shows the element–partial DOS curve for $Li_{15}Si_4$ and its decomposition into the orbital momentum contribution in the top panel. The top panel in Fig. 3 is the

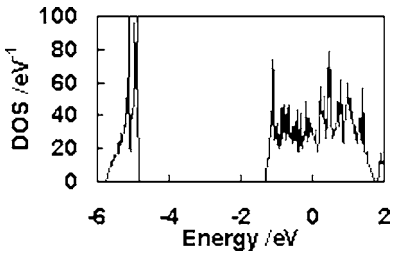

FIG. 2. The total DOS curve for $Li_{15}Si_4$. The energy scale is relative to the Fermi level.

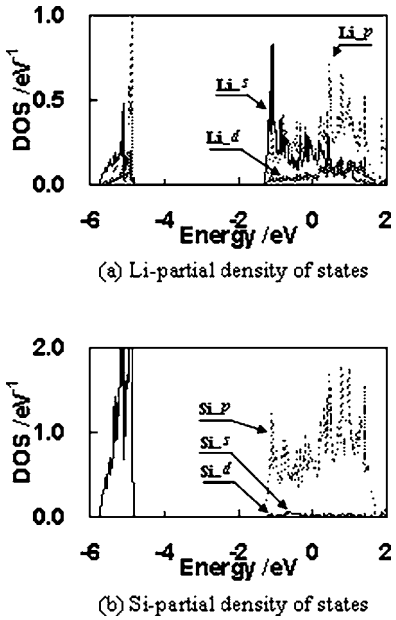

FIG. 3. (a) The Li-partial DOS curve for $Li_{15}Si_4$ and its decomposition into orbital momentum contribution. (b) The Si-partial DOS curve for $Li_{15}Si_4$ and its decomposition into orbital momentum contribution. The energy scale is relative to the Fermi level.

DOS curve for Li, and the bottom is the DOS curve for Si. The energy scale is relative to E_F. Both Li and Si have band gaps as well as total DOS. It is found that the states for Li in $Li_{15}Si_4$ are mainly made of *s* and *p* characters, and there is a slight appearance of a *d* character. For Si in $Li_{15}Si_4$, the states are mainly made of a *p* character from E_F to −1.3 eV, and the intensity of the *s* character reverses that of the *p* character from −4.9 eV to −5.7 eV.

Considering the electron densities and DOS curves, we think that the electron transfer from electrons with *p* and *d* symmetries in the Si atoms in crystalline Si to electrons with *p* and *d* symmetries in the Li atoms in $Li_{15}Si_4$ occurs during the Li intercalation reaction for Si anodes.

C. Average Li intercalation voltage

Next, we calculate the average intercalation voltage from the total energy difference between the sum of metallic Li and crystalline Si and $Li_{15}Si_4$. Since the total energy of $Li_{15}Si_4$, including 60 Li atoms and 16 Si atoms in a unit cell is −218.644 eV, $E_r[Li_{15/4}Si]=13.665$ eV per one $Li_{15/4}Si$. On the other hand, $E_r[Li]=-1.897$ eV per one metallic Li and $E_r[Si]=-5.414$ eV per one crystalline Si.[40] By assigning $x=0$, $y=15/4$ to Eq. (1), the Gibbs free energy change in the Li intercalation reaction of $Li_{15}Si_4$ is

$$\Delta G_r = \Delta E_r = E_r[Li_{15/4}Si] - 15/4\ E_r[Li] - E_r[Si] = -1.136\ \text{eV}.$$

By applying the Gibbs free energy change to Eq. (2), we obtain the average intercalation voltage of 0.303 V.

It is known that the lithiation of crystalline Si provides the amorphous Li–Si alloy in a voltage plateau region during the discharge.[12–14] We cannot obtain the average intercalation voltage for the amorphous Li–Si alloy system since it is difficult to express the amorphous Li–Si alloy within the framework of DFT calculations. Therefore, the calculated average intercalation voltage is quantitatively evaluated by another method.

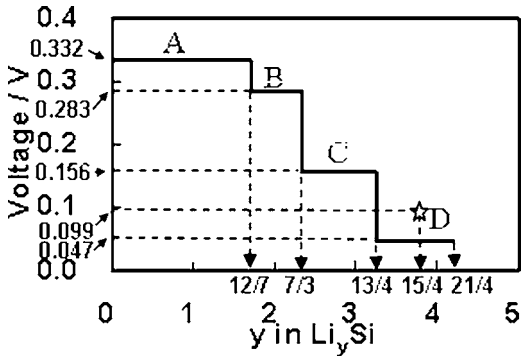

FIG. 4. Schematic OCV curve of a Si electrode in the LiCl–KCl eutectic melt at 688 K reported in Ref. 16.

Figure 4 shows a schematic OCV curve of crystalline Si electrode in a LiCl–KCl eutectic melt at 688 K by use of the Coulometric titration technique reported by Wen and Huggins.[16] Four voltage plateaus of *A*–*D* are attributed to the formation of various types of Li–Si alloys. It is known that four Li–Si compound phases, $Li_{12}Si_7$, Li_7Si_3, $Li_{13}Si_4$, and $Li_{21}Si_5$, and a liquid phase exist at this temperature. The formation of $Li_{12}Si_7$, Li_7Si_3, $Li_{13}Si_4$, and $Li_{21}Si_5$, and the liquid phases occurs at four voltage plateaus of *A*–*D*, as represented by the following reaction formulas (4)–(7):

$$\text{Si} + 12/7\ \text{Li} \rightarrow \text{Li}_{12/7}\text{Si}, \tag{4}$$

$$\text{Li}_{12/7}\text{Si} + 13/21\ \text{Li} \rightarrow \text{Li}_{7/3}\text{Si}, \tag{5}$$

$$\text{Li}_{7/3}\text{Si} + 11/12\ \text{Li} \rightarrow \text{Li}_{13/4}\text{Si}, \tag{6}$$

$$\text{Li}_{13/4}\text{Si} + 19/20\ \text{Li} \rightarrow \text{Li}_{21/5}\text{Si}. \tag{7}$$

Here we replace reaction formula (7) in Fig. 4(d) by

$$\text{Li}_{13/4}\text{Si} + 1/2\ \text{Li} \rightarrow \text{Li}_{15/4}\text{Si}. \tag{8}$$

This replacement may be far from reality since the voltage plateau of the coexistence of $Li_{15/4}Si$ and crystalline Si has not been found in the Coulometric titration experiment. However, if the coexistence of $Li_{15/4}Si$ and crystalline Si exists, the voltage should be approximately the point midway between the voltage under the coexistence of $Li_{13/4}Si$ and crystalline Si (0.156 V) and that under the coexistence of $Li_{21/5}Si$ and crystalline Si (0.047 V) since 15/4 is approximately equal to the value between 13/4 and 21/5. Therefore, we obtain 0.099 V as an OCV of the coexistence of $Li_{15/4}Si$ and crystalline Si. By transforming Eq. (3), the following internal energy of Li_ySi in reaction formula (1) is expressed by

$$E_r^{\text{expt}}[\text{Li}_y\text{Si}] = E_r^{\text{expt}}[\text{Li}_x\text{Si}] + (y-x)E_r^{\text{expt}}[\text{Li}] - (y-x)F\bar{V}. \tag{9}$$

By applying Eq. (9) to reaction formulas (4)–(7) and summing them, we obtain

$$E_r^{\text{expt}}[\text{Li}_{15/4}\text{Si}] = E_r^{\text{expt}}[\text{Si}] + \frac{15}{4}E_r^{\text{expt}}[\text{Li}] - F\left(0.332 * \frac{12}{7} + 0.283 * \frac{13}{21} + 0.156 * \frac{11}{12} + 0.099 * \frac{1}{2}\right). \quad (10)$$

Now we define the experimental average intercalation voltage as

$$\bar{V}^{\text{expt}} = \frac{E_r^{\text{expt}}[\text{Si}] + 15/4E_r^{\text{expt}}[\text{Li}] - E_r^{\text{expt}}[\text{Li}_{15/4}\text{Si}]}{15F/4}. \quad (11)$$

By transforming Eq. (10), we obtain $\bar{V}^{\text{expt}}=0.250$ V.

It is found that this voltage is close to the average intercalation voltage calculated by using DFT calculations in spite of replacing $Li_{21/5}Si$ by $Li_{15/4}Si$ in a voltage transient curve of crystalline Si. Therefore, we think that the average intercalation voltage of 0.303 V is appropriate for the Li–Si system.

IV. CONCLUSION

We investigated the electronic structure of $Li_{15}Si_4$, which appears at the bottom of the discharge for crystalline Si and amorphous Si anodes of LIBs by using DFT calculations. $Li_{15}Si_4$ is formed by a unit figure in which six Li atoms surround a Si atom with two different Li–Si bond lengths. The series of the unit figures intricately intersect with other series of the unit figures. The closest Li–Li bond length in $Li_{15}Si_4$ is much shorter than that in metallic Li. We attribute the short Li–Li bond length in $Li_{15}Si_4$ to forcing the Li atoms to cage in the Li–Si alloy cavities. The Li–Si bond lengths in $Li_{15}Si_4$ are close to the average bond length calculated by using the Si–Si bond length in crystalline Si and the Li–Li bond length in metallic Li. Contrary to the common belief that the Li atom is regarded as a cation in the electrode materials, the Li atom in $Li_{15}Si_4$ is an anion with an excess charge of 0.56–0.63 from the electron densities and DOS curves. The electrons in $Li_{15}Si_4$ are mainly distributed to the Si atoms due to electronegativity. The charge densities at the bonding midpoints of the Li–Si bonds are much higher than those in Li–Li bond. The electrons in the Si atom contribute to the formation of the Li anions. The average intercalation voltage of about 0.3 V is obtained in Si anodes of LIBs. The comparison between the voltage calculated by DFT calculations and that predicted from the open-circuit voltage curve for Li–Si alloys shows excellent agreement.

ACKNOWLEDGMENTS

This work is supported by the Ministry of Education, Culture, Sports, Science and Technology of Japan (MEXT) through their Grant-in-Aid for Scientific Research on Priority Areas (Developing Next Generation Quantum Simulators and Quantum-Based Design Techniques) and Special Coordination Funds for the 21st Century Center of Excellence (COE) Program (G18) "Core Research and Advance Education Center for Materials Science and Nano-Engineering". Some of the calculations were done using the computer facilities of the Cybermedia Center (Osaka University), the ISSP Super Computer Center (University of Tokyo), the Yukawa Institute (Kyoto University), and the Japan Atomic Energy Research Institute (ITBL, JAERI).

[1] *Lithium Batteries Science and Technology*, edited by G.-A. Nazri and G. Pistoia (Kluwer Academic, New York, 2004), p. 113.
[2] J. M. Tarascon and M. Armand, Nature **414**, 359 (2001).
[3] J. R. Dahn, T. Zheng, Y. Liu, and J. S. Xue, Science **270**, 590 (1995).
[4] R. A. Sharma and R. N. Seefurth, J. Electrochem. Soc. **123**, 1763 (1976).
[5] B. A. Boukamp, G. C. Lesh, and R. A. Huggins, J. Electrochem. Soc. **128**, 725 (1981).
[6] J. Yang, M. Winter, and J. O. Besenhard, Solid State Ionics **90**, 281 (1996).
[7] R. A. Huggins, Solid State Ionics **113-115**, 57 (1998).
[8] M. Winter and J. O. Besenhard, Electrochim. Acta **45**, 31 (1999).
[9] R. A. Huggins, J. Power Sources **81-82**, 13 (1999).
[10] H. Li, X. Huang, L. Chen, G. Zhou, Z. Zhang, D. Yu, Y. J. Mo, and N. Pei, Solid State Ionics **135**, 181 (2000).
[11] J. P. Maranchi, A. F. Hepp, and P. N. Kumta, Electrochem. Solid-State Lett. **6**, A198 (2003).
[12] M. N. Obrovac and L. Christensen, Electrochem. Solid-State Lett. **7**, A93 (2004).
[13] P. Limthongkul, Y. I. Jang, N. J. Dudney, and Y. M. Chiang, J. Power Sources **119-121**, 604 (2003).
[14] P. Limthongkul, Y. I. Jang, N. J. Dudney, and Y. M. Chiang, Acta Mater. **51**, 1103 (2003).
[15] T. D. Hatchard and J. R. Dahn, J. Electrochem. Soc. **151**, A838 (2004).
[16] C. J. Wen and R. A. Huggins, J. Solid State Chem. **37**, 271 (1981).
[17] C. van der Marel, G. J. B. Vinke, and W. V. D. Lugt, Solid State Commun. **54**, 917 (1985).
[18] R. Nesper and H. G. von Schnering, J. Solid State Chem. **70**, 48 (1987).
[19] U. Frank, W. Müller, and H. Schäfer, Z. Naturforsch. B **30**, 10 (1975).
[20] H. G. von Schnering, R. Nesper, K. F. Tebbe, and J. Curda, Z. Metallkd. **71**, 357 (1980).
[21] R. Nesper, H. G. von Schnering, and J. Curda, Chem. Ber. **119**, 3576 (1986).
[22] H. G. von Schnering, R. Nesper, J. Curda, and K.-F. Tebbe, Angew. Chem. Int. Ed. Engl. **19**, 1033 (1980).
[23] J. Evers, G. Oehlinger, and G. Sextl, Angew. Chem. Int. Ed. Engl. **32**, 1442 (1993).
[24] L. A. Stearns, J. Gryko, J. Diefenbacher, G. K. Ramachandran, and P. F. McMillan, J. Solid State Chem. **173**, 251 (2003).
[25] J. Chouvin, J. Olivier-Fourcade, J. C. Jumas, B. Simon, and O. Godiveau, Chem. Phys. Lett. **308**, 413 (1999).
[26] C. J. Wen and R. A. Huggins, J. Electrochem. Soc. **128**, 1181 (1981).
[27] M. K. Aydinol and G. Ceder, J. Electrochem. Soc. **144**, 3832 (1997).
[28] M. K. Aydinol, A. F. Kohan, G. Ceder, K. Cho, and J. Joannopoulos, Phys. Rev. B **56**, 1354 (1997).
[29] I. A. Courtney, J. S. Tse, O. Mao, J. Hafner, and J. R. Dahn, Phys. Rev. B **58**, 15583 (1998).
[30] D. Vanderbilt, Phys. Rev. B **41**, 7892 (1990).
[31] G. Kresse and J. Hafner, J. Phys.: Condens. Matter **6**, 8245 (1994).
[32] G. Kresse and J. Hafner, Phys. Rev. B **47**, 558 (1993).
[33] G. Kresse and J. Hafner, Phys. Rev. B **49**, 14251 (1994).
[34] G. Kresse and J. Furthmüller, Comput. Mater. Sci. **6**, 15 (1996).
[35] G. Kresse and J. Furthmüller, Phys. Rev. B **54**, 11169 (1996).
[36] J. P. Perdew, K. Burke, and M. Ernzerhof, Phys. Rev. Lett. **77**, 3865 (1996).
[37] J. P. Perdew, K. Burke, and M. Ernzerhof, Phys. Rev. Lett. **78**, 1396 (1997).
[38] M. P. Teter, M. C. Payne, and D. C. Allan, Phys. Rev. B **40**, 12255 (1989).
[39] D. M. Bylander, L. Kleinman, and S. Lee, Phys. Rev. B **42**, 1394 (1990).
[40] Y. Kubota, M. C. S. Escaño, H. Nakanishi, and H. Kasai, J. Alloys Compd. (in press).
[41] H. V. Leuken, G. A. de Wijs, W. V. D. Lugt, and R. A. de Groot, Phys. Rev. B **53**, 10599 (1996).